HHS Public Access

Author manuscript

Biochemistry. Author manuscript; available in PMC 2019 April 10.

Published in final edited form as:

Biochemistry. 2018 April 10; 57(14): 2150–2161. doi:10.1021/acs.biochem.7b01194.

Cytochrome aa_3 oxygen reductase utilizes the tunnel observed in the crystal structures to deliver O_2 for catalysis

Paween Mahinthichaichan[‡], **Robert B. Gennis**[*,§], and **Emad Tajkhorshid**[*,‡]

[‡]Department of Biochemistry, NIH Center for Macromolecular Modeling and Bioinformatics, Beckman Institute for Advanced Science and Technology, University of Illinois at Urbana-Champaign, Urbana, IL 61801, U.S.A.

[§]Department of Biochemistry, University of Illinois at Urbana-Champaign, Urbana, IL 61801, U.S.A.

Abstract

Cytochrome aa_3 is the terminal respiratory enzyme of all eukaryotes and many bacteria and archaea, reducing O_2 to water and harnessing the free energy from the reaction to generate the transmembrane electrochemical potential. The diffusion of O_2 to the heme-copper catalytic site, which is buried deep inside the enzyme, is the initiation step of the reaction chemistry. Our previous molecular dynamics (MD) study with cytochrome ba_3, a homologous enzyme of cytochrome aa_3 in *Thermus thermophilus*, demonstrated that O_2 diffuses from the lipid bilayer to its reduction site through a 25-Å long tunnel inferred by Xe-binding sites detected by X-ray crystallography.[1] Although a similar tunnel is observed in cytochrome aa_3, this putative pathway appears partially occluded between the entrances and the reduction site. Also, the experimentally determined second-order rate constant for O_2 delivery in cytochrome aa_3 ($\sim 10^8$ $M^{-1}s^{-1}$) is 10 times slower than that in cytochrome ba_3 ($\sim 10^9$ $M^{-1}s^{-1}$). A question to be addressed is whether cytochrome aa_3 utilizes this X-ray inferred tunnel as the primary pathway for O_2 delivery. Using complimentary computational methods including multiple independent flooding MD simulations and implicit ligand sampling calculations, we probe the O_2 delivery pathways in cytochrome aa_3 of *Rhodobacter sphaeroides*. All of the O_2 molecules that arrived in the reduction site during the simulations were found to diffuse through the X-ray observed tunnel, despite its apparent constriction, supporting its role as the main O_2 delivery pathway in cytochrome aa_3. The rate constant for O_2 delivery in cytochrome aa_3, approximated using the simulation results, is 10 times slower than in cytochrome ba_3, in agreement with the experimentally determined rate constants.

Table of Contents

r-gennis@illinois.edu; emad@life.illinois.edu, Phone: +1 217 3339075; +1 217 2446914.

Supporting Information **Available**

Included in the Supporting Information are the distributions of atomic partial charges assigned to the heme cofactors (Fig. S1), the observed conformations of key amino acid residues at the main barrier of the O_2 delivery pathway (Fig. S2), and the comparisons of O_2 models used in the flooding simulations and ILS calculations (Fig. S1–S4 and Table 1). The comparisons of the slightly charged O_2 model, in which the oxygen atoms contain the partial charges of ±0.021, and apolar model, in which the atoms contain the partial charges of 0, were done by calculating the solvation free energies (Table S1), the interactions between O_2 and water molecules depited by the pairwise distribution or g(r) (Fig. S3) and the partitioning profiles of O_2 in the membrane and in the aqueous solution (Fig. S4).

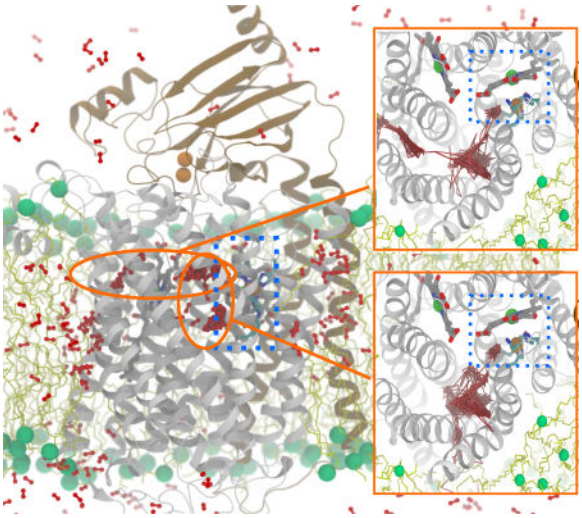

Introduction

A-family heme-copper oxygen reductases (HCOs) including the aa_3-type cytochrome c oxidases (cytochrome aa_3) are the terminal respiratory oxygen reductases of all eukaryotes and many bacteria and archaea.[2–5] These enzymes oxidize cytochrome *c* and reduce O_2 to water, and use the free energy from the O_2 reduction reaction to power the biosynthesis of ATP.[6–12] The atomic structures of cytochrome aa_3 from *Rhodobacter sphaeroides* (*R.s*),[13,14] *Paracoccus denitrificans*[15] and bovine heart mitochondria[16–19] have been determined by X-ray crystallography. The bacterial enzymes comprise 3–4 subunits (Fig. 1A), whereas the mitochondrial enzymes contain at least ten additional accessory subunits.[20,21] The smaller bacterial enzymes are widely used as models for the mitochondrial enzymes. A homologue of cytochrome aa_3 is cytochrome bo_3 of *E. coli*,[5,22,23] which uses ubiquinol instead of cytochrome *c* as the electron donor.

The reduction of O_2 takes place in Subunit I (SI), a 12-TM helical subunit, containing heme *a* and the O_2 reduction site composed of heme a_3 and Cu_B (Fig. 1A). The reaction requires four electrons and eight protons, of which four are for the reduction of O_2 and four are translocated across the membrane.

$$O_2 + 8H^+_{N,\,chem,\,pump} + 4e^- \rightarrow 2H_2O + 4H^+_{P,\,pump}$$

The four electrons are provided by the sequential oxidation of four cytochrome c^{red} molecules by the one-electron redox center Cu_A located in the periplasmic domain of Subunit II (SII). Electrons are sequentially shuttled to heme *a* and then to the reduction site. All of the protons come from the N (electrically negative) side of the membrane and are transferred via two proton-conducting input channels, the D and K channels.[8,20] The D channel transfers two of the chemical protons and all of the pumped protons. It is 25–30 Å long and comprises a continuous hydrogen-bonded network formed by water molecules and conserved polar amino acids linking residue D132 (numbering for the *R. sphaeroides*

enzyme) anchored on the surface of the N side and residue E286 located near heme *a* and the reduction site. The K channel, which transfers two chemical protons, begins at residue E101 in SII and includes residue K362 near the SI–SII interface. The two channels are not redundant, each providing chemical protons during different steps in the catalytic cycle. Starting with a fully reduced enzyme, the binding of O_2 to heme a_3 initiates the O_2 reduction chemistry and reaction steps associated with proton pumping. The O_2 delivery pathway, however, has not been well characterized and is the topic of the current work.

A previous MD study from this laboratory with a B-family HCO, cytochrome ba_3 from *Thermus thermophilus*[1] demonstrated that O_2 diffuses from the lipid bilayer to the reduction site through a hydrophobic tunnel that is the same as that defined by Xe-binding sites observed in the crystal structure of the protein (Fig. 1D).[24,25] This tunnel is also apparent in the absence of bound Xe in all of the available crystal structures of cytochrome ba_3.[26–28] The O_2 delivery pathway in cytochrome ba_3 has two entrances enabling O_2 access to the protein from the lipid bilayer. Both entrances begin at SI-lipid interfaces (Fig. 1D); one (termed TM1–3) is spanned by TM1, TM2 and TM3 helices, and other (termed TM4–5) is spanned by TM4 and TM5 helices. This structural feature is a "static" tunnel and is referred to as the "X-ray inferred" pathway.

An equivalent tunnel with the same two entrances (Fig. 1A–C) is observed in the crystal structures of the A-family oxygen reductases including cytochrome aa_3 from different sources.[13,19,24,29–31] However, in the A-family enzymes, these tunnels appear to be partially occluded (Fig. 1B–C), consistent with the experimental apparent second order rate constant for O_2 diffusion from the aqueous solution to the reduction site of cytochrome aa_3 (10^8 $M^{-1}s^{-1}$) being 10 times slower than for cytochrome ba_3.[32,33]

The A-family oxygen reductases have a 7-TM helical subunit III (SIII) that is not present in cytochrome ba_3 or other B-family HCOs, and the TM4–5 entrance of the putative O_2 pathway in SI is adjacent to SIII. However, there are no data that indicate a functional role of SIII in O_2 delivery to the reduction site that might result from its proximity to the tunnel entrance. Although the elimination of SIII has deleterious effects, the A-family enzymes remain functional.[8,34–37] X-ray structures of A-family HCOs without SIII indicate no structural perturbations to SI or SII or to the O_2 pathways[14,15,38–40] (Fig. 1B–C).

Two MD studies have, however, reached opposite conclusions about the use of the X-ray inferred tunnel by O_2 to reach the reduction site in the A-family HCOs. An early (1998) MD study by the Schulten group[41] applied the locally enhanced sampling (LES) technique[42] to simulate O_2 diffusion in cytochrome aa_3 oxygen reductases from *P. denitrificans* (*P.d*) and bovine. They observed an O_2 molecule initially placed at the reduction site exiting via the entrance of the X-ray inferred tunnel in each case. However, these LES simulations[41] were performed in vacuum and lasted only several picoseconds. Because LES accelerates O_2 diffusion by softening interactions between O_2 and its surroundings, it might not correctly capture the dynamics that are functionally relevant for O_2 delivery.

More recently, an MD study of the A-family *R.s.* cytochrome aa_3 by Oliveira et al[43] probed the O_2 delivery pathway by performing five 100-ns flooding simulations, in which multiple

copies of O_2 were explicitly included and simulated with the rest of the system (i.e. protein, lipids, water and ions). Unlike LES, flooding simulation is based on equilibrium, conventational simulations with no perturbation and rescaling of interactions between atoms in the system. However, no O_2 entry was observed during these simulations. They performed energy estimations using the implicit ligand sampling (ILS) technique, a post-simulation analysis used in probing high affinity O_2 sites,[44] and the results suggested two alternate dynamically formed tunnels as preferred O_2 pathways over the X-ray inferred tunnel.

Experimental mutagenesis data which support the use of the X-ray inferred tunnel as the O_2 delivery pathway in the A-family HCOs are based on amino acid residues, such as V279 of *P.d.* cytochrome aa_3[45] and V287 of *E. coli* cytochrome bo_3[46] (equivalent to V287 *R.s.* cytochrome aa_3), that are located very close to the reduction site rather than within the tunnel. Also, although an X-ray crystallographic experiment detected two Xe binding sites in the *R.s.* enzyme,[13] those sites are located near the entrances of the pathway and therefore do not necessarily define a clear pathway for O_2 delivery.

Since the two previous MD simulations for O_2 diffusion to the reduction site of A-family oxygen reductases arrived at different conclusions, the present study re-examines the issue by independently performing both ILS analyses and an extended set of flooding simulations of the diffusion of O_2 to the reduction site of the *R.s.* cytochrome aa_3. The X-ray model used for the simulations includes SI and SII (Fig. 2). To improve the statistics on the O_2 delivery pathways compared to previous studies, twenty independent flooding simulations with different starting points were performed and each was extended to 150 ns. ILS analyses were performed on an independent 200-ns MD simulation. The results clearly show that the only pathway used by O_2 to reach the reduction site is the X-ray inferred tunnel, similar to what has been shown for the B-family cytochrome ba_3 from *T. thermophilus* (*T.t.*[1] Constrictions along the pathway result in a rate of O_2 delivery that is at least 10 times slower than the rate observed[32,33] and calculated[1] for cytochrome ba_3.

Methods and Materials

System preparation

The membrane-embedded model of *R.s.* cytochrome aa_3 was prepared using the 2.0-Å crystal structure (PDB 2GSM) as the protein model. The structure comprises SI (catalytic subunit), which binds low-spin heme *a*, high-spin heme a_3 and Cu_B cofactors, SII, which binds the Cu_A complex, and 282 water molecules. Hydrogen atoms were added using PSFGEN in VMD.[48] Histidine residues except H102, H333, H334, H411, H419 and H421 of SI were in the HSE tautomeric form (N_ε atom of the imidazole ring carrying proton). H102 and H421 are ligated to the Fe atom of heme *a*, H284, H333 and H334 are ligated to Cu_B, H419 is ligated to the Fe atom of heme a_3, and H411 forms a hydrogen bond with the propionate A of heme a_3. The carboxylate side chain of residue E286, for which pK_a has been experimentally estimated to be >9,[49] was assigned to be protonated.

The first principal axis of the protein was aligned with the z axis (membrane normal) using the OPM (Orientations of Proteins in Membranes) database.[50,51] The protein was then inserted into a patch of POPE (1-palmitoyl-2-oleoyl-sn-glycero-3-phosphoethanolamine)

bilayer. Lipids that overlapped the protein were removed, keeping 132 lipids in the periplasmic and cytoplasmic leaflets. The membrane-embedded enzyme complex was then solvated with water. Water molecules that were in the membrane ($-18 < z < 18$), except those from the crystal structure, were removed, keeping 20,637 water molecules. Finally, 0.2 M NaCl (78 Na^+ and 79 Cl^- ions) was added to neutralize and ionize the system, resulting in a fully solvated model of 104,710 atoms.

The CHARMM22 force field with ϕ/ψ corrections[52,53] was used to describe the protein and the heme cofactors, CHARMM36[54] for the lipids, and the TIP3P model[55] for water molecules. The cofactors were treated in the reduced state. The partial charge of 0.383 was used for Cu_B according to Hofacker and Schulten.[41] The vdW parameters of Cu with ε = 0.19 kcal/mol and R_{min} =1.4 Å were from Fuchs et al.[56] The force field parameters for the hydroxyethylfarnesyl side chain, attached to the porphyrin ring of hemes *a* and a_3, were not available in the CHARMM force field library; they were constructed by analogy using parameterized alcohol, aldehyde, alkene, and alkane fragments;[57] the complete structure of the hemes with the atomic partial charges is shown in Fig. S1. For the Cu_A complex, the partial charges of its Cu atoms and its ligated amino acids were assigned according to Hofacker and Schulten.[41]

Simulation protocols

MD simulations performed to prepare the systems consisted of the following steps: (1) 0.5-ns melting of lipid tails during which only the lipid tails were allowed to move in order to achieve better packing of lipids around the inserted protein; (2) 0.5-ns simulation with restraints (k = 1 kcal/mol/Å^2) applied to heavy atoms of the protein and cofactors (all lipid atoms and water moving) and with harmonic potentials (k = 0.1 kcal/mol/Å^2) applied to keep water out of the membrane; (3) 0.5-ns simulations with only backbone atoms of the protein and heavy atoms of the cofactors restrained (k = 1 kcal/mol/Å^2); (4) 1-ns simulation with only C_α atoms of the protein and heavy atoms of the cofactors restrained; and (5) 20-ns unrestrained relaxation. Energy minimization (1,000 steps) was performed at the beginning of Steps 1, 2 and 3 using the conjugate gradient algorithm. To maintain the ligation of Cu_B to H284, H333 and H334 and thereby the structure of the reduction site, the His-Cu_B, and heme a_3 Fe-Cu_B connections were described by bonded interactions (k =200 kcal/mol/Å^2 for bonds and k =50 kcal/mol/rad^2 for angles).

All simulations were performed using NAMD2[58] with a time step of 2 fs and with the periodic boundary condition (PBC). All bonds involving hydrogen atoms were kept rigid using the SHAKE algorithm.[59] To evaluate long-range electrostatic interactions in PBC without truncation, the particle mesh Ewald (PME) method[60] with a grid density of 1/Å^3 was used. The cutoff for van der Waals interactions was set at 12 Å. All of simulation steps except the melting of lipid tails (Step 1) were performed in a flexible cell, which allows the system to change its dimensions independently as an NPT ensemble. The temperature was maintained at 310 K by Langevin dynamics[61] with a damping coefficient γ of 1 /ps. The Nosé-Hoover Langevin piston method[61,62] with a piston period of 200 fs was used to maintain the pressure at 1 atm.

Production runs

The production runs consist of a 200-ns apo simulation performed in the absence of O_2 molecules (used for ILS analysis and starting flooding simulations), and a set of twenty 150-ns flooding simulations in which a large number of O_2 molecules were added. The apo simulation started from the 20-ns time point of the relaxation simulation. The set of twenty flooding simulations started from snapshot taken at different time points from the 200-ns apo simulation described above: 4 snapshots (at 25-ns, 100-ns, 150-ns, and 200-ns time points, respectively) were selected from the apo simulation and each one were used to seed 5 indepedent simulations, resulting in an ensemble of twenty simulations.

Flooding simulations

Flooding simulations were carried out to probe potential O_2 delivery pathways and the dynamics associated with the O_2 delivery process. To maximize the sampling of O_2 delivery pathways within a limited timescale (150 ns), 130 O_2 molecules, corresponding to a concentration of 210 mM with respect to the volume of the simulation box, were added to the equilibrated structure of the membrane-embedded cytochrome aa_3. At the start of the simulation, 70 O_2 molecules were placed in the membrane and 60 molecules in the aqueous phas generating a concentration of 185 mM in the aqueous phase with all O_2 molecules occupying space outside the protein (Fig. 2). Twenty 150-ns simulations, adding upto a total of 3,000 ns, were carried out to probe for potential O_2 pathways. The simulated O_2 molecules are described by the standard CHARMM force field.[52] The partial charges for the oxygen atoms of O_2 are +0.021 and −0.021, respectively. Its intramolecular interactions are described by the bond distance of 1.23 Å and the spring constant of 600 kcal/mol/Å^2. The vdW parameters of the oxygen atoms are with ε = −0.12 kcal/mol and R_{min} =1.7 Å. We note that the O_2 model with the partial charges of ±0.021 and the one with the partial charges of 0 used in the ILS calculations, in which no electrostatic terms are included, show negligible differences in O_2 solvation in the aqueous solution and O_2 partitioning in the membrane (Fig. S3–S4 and Table S1). Moreover, it is important to note that although the phrase "O_2 ligand for heme" is tagged in the CHARMM topology file containing both O_2 and hemes, these charges of ±0.021 are far away from the strongly polarized O_2 molecule when ligated to the heme iron. A calculation by Daigle et al[63] showed that oxygen atoms of an O_2 molecule ligated to heme are strongly polarized with the partial charges of −0.18 and −0.32, clearly indicating that the slightly charged model (±0.021) used in the flooding simulations is not representing a heme-bound O_2. The very small charges of ±0.021 used in the present study (and in other simulation studies[64,65]) are used to take into account a portion of the polarization that O_2 would experience when it approaches to strongly charged portions of the protein. In such cases, the rotation of O_2 can orient the small introduced dipole with the surrounding field, thereby giving a small portion of polarization effects.

To identify whether O_2 delivery events took place during the simulations, we used the 6-Å distance cutoff from Cu_B as the criterion. Then, we obtained the identity of the delivered O_2 molecules and examined the simulation trajectories whether they were indeed localized in the reduction site.

Implicit ligand sampling (ILS)

Complementary to the flooding simulations in which ligand diffusion is explicitly probed, ILS was employed to identify potential regions and pathways for O_2 insertion that may not be sufficiently sampled by flooding simulaitons. ILS calculates ligand-interaction energies (E_i) in any position inside the protein over an ensemble of protein conformations and ligand orientations,[44] which estimate a 3D free energy map of inserting an O_2 molecule at position i (ΔG_i).

$$\Delta G_i = -RT \ln \frac{p_i}{p_0} = -RT \ln \frac{< e^{-E_i/RT} >}{p_0}$$

where p_0 (in vacuum) = 1 and p_i is the probability of inserting an O_2 molecule at position i.

Following the assumption that small, hydrophobic gases weakly interact with proteins and therefore do not affect the protein structure and dynamics, the 200-ns apo trajectory (10,000 frames) was analyzed for O_2 pathways. O_2 molecules were sampled in a 55 × 50 × 75 $Å^3$ grid with spacing of 1 Å, covering the entire cytochrome aa_3 enzyme. Ten orientations of O_2 were sampled in each subgrid, which contained 3×3×3 interaction sites. The solvation free energy of O_2 (ΔG_{sol}) was used as the reference for calculating the partitioning free energy of O_2 ($\Delta G_{i,sol}$).

$$\Delta G_{i,sol} = \Delta G_i - \Delta G_{sol}$$

ΔG_{sol} was independently calculated over a 30×30×30 $Å^3$ using of NaCl solution ILS and free-energy perturbation (FEP).[66] Both techniques yield ΔG_{sol} values of 2.1 kcal/mol, which is consistent to a previous calculation by Cohen et al.[44]

Results and Discussion

O_2 delivery pathway to the reduction site

To unequivocally probe for pathways used by O_2 to diffuse to the reduction site of cytochrome aa_3, flooding simulations with 130 O_2 molecules were performed. Twenty simulations were performed using different starting points taken from the equilibrated system of the apo simulation: at t = 25 ns, 100 ns, 150 ns or 200 ns. The O_2 molecules were initially placed outside the protein, 70 molecules in the membrane and 60 molecules in the aqueous solution. Each simulation lasted 150 ns, but it took only ~20 ns to achieve steady distributions of O_2 in both the membrane and aqueous phases (Fig. 2), where ~110 O_2 molecules resided in the membrane and ~20 resided in the aqueous solution. In 15 of 20 simulations, O_2 molecules were observed to enter the reduction site; the number of this event ranged from 1 to 7 with an average of 2 events per simulation, corresponding to an average of O_2 entry in every 75 ns. Based on the 6-Å distance cutoff from the center of Fe of heme a_3 and Cu_B, the residence times of O_2 in the reduction site ranged from ~1 ns to ~90 ns (Fig. 3).

O_2 molecules that reached the reduction site were identified and their diffusion dynamics was visually examined in order to locate the O_2 delivery pathways. Their trajectories are shown in Fig. 4; each colored line represents an individual O_2 molecule. The results of flooding simulations showed that the delivered O_2 molecules enter the reduction site via a pathway, which contains three entry branches (entrances) accessible from the membrane. One of the entrances begins at a lipid-protein interfacial region formed by TM1, TM2 and TM3 (TM1–3) helices, one begins at the TM4–TM5 (TM4–5) interface, and one begins at the TM5–TM6 (TM5–6) interface. In some of the simulations, O_2 is observed to enter via all three entrances, while in others, the entries occur via only one or two entrances (Fig. 4). The location of the pathway in cytochrome aa_3 is similar to the one previously defined for O_2 delivery in cytochrome ba_3, which resembles a Y-shaped tunnel (shown in Fig. 1C). The O_2 delivery pathway in cytochrome ba_3[1] corresponds to a two-branched hydrophobic tunnel as was also determined to bind Xe by X-ray crystallography.[24,25] The TM1–3 entrance of cytochrome aa_3 is equivalent to Branch A of cytochrome ba_3, so it is referred to as Branch A. The TM4–5 entrance is equivalent to Branch B, so it is referred to as Branch B. The TM5–6 entrance was not found in cytochrome ba_3 and is denoted as Branch C.

Comparisons of O_2 delivery pathways in cytochrome aa_3 and cytochrome ba_3

The slower O_2 delivery rate in cytochrome aa_3 (1×10^8 $M^{-1}s^{-1}$) compared to the one in cytochrome ba_3 (1×10^9 $M^{-1}s^{-1}$)[32,33] is probably due to the presence of diffusions barriers within the protein. However, the inability to observe O_2 delivery in some of the flooding simulations makes it difficult to compare our current results with cytochrome aa_3 and our previous ones with cytochrome ba_3 using the results of flooding simulations. Therefore, ILS analyses were performed to calculate thermodynamically favorable O_2 regions within cytochrome aa_3. The results of ILS were used to map out potential O_2 delivery pathways, which were then compared to the pathways obtained from the flooding simulations and to the results of cytochrome ba_3 obtained from our previous study.[1] The comparison between cytochrome aa_3 and cytochrome ba_3 is shown in Fig. 5A–B as 3D free energy isosurfaces, in which the colored surfaces represent free energy states of O_2 insertion.

For cytochrome ba_3, the entire O_2 delivery pathway is energetically favorable as indicated in Fig 5B by the Y-shaped red surface corresponding to ΔG of −3.3 kcal/mol. For cytochrome aa_3, the pathway identified by the flooding simulations are found to be less favorable for O_2 insertion relative to the one in cytochrome ba_3. The pathway contains several higher energy regions between the entrances and the reduction site illustrated in Fig 5A by the discontinuity of the magenta surfaces corresponding to ΔG of −1.8 kcal/mol forming diffusion barriers. Here, O_2 molecules diffusing from any of the three entrances to the reduction site encounter a barrier located in the vicinity of residues F172 and G283.

In both cytochrome aa_3 and cytochrome ba_3, the results of flooding simulations are correlated to the results of ILS calculations. In our previous study of O_2 delivery in cytochrome ba_3, although flooding simulations were performed for only 50 ns using the O_2 concentration of 210 mM, we were able to observe O_2 delivery on an average of 20 events.[1] For cytochrome aa_3, the simulations lasted much longer (150 ns), but only two delivery events occurred on the average, which represent a 30-fold decrease compared to cytochrome

ba$_3$. Fewer O_2 delivery events indicate that the pathway in cytochrome *aa*$_3$ is less accessible to O_2 than the one in cytochrome *ba*$_3$.

The study by Oliveira et al[43] with the same *R.s.* cytochrome *aa*$_3$ presented five 100-ns flooding simulations but found no O_2 entry. These results are consistent with the present study insofar we also found free energy barriers that limit the rate of O_2 diffusion to the reduction site. Five of the 20 simulations performed in the present study exhibited no O_2 entry events while the rest observed only few events (Table 1). Based on their ILS analyses, however, Oliveira et al[43] concluded that O_2 prefers to use alternate pathways rather than the X-ray inferred pathway to reach the reduction site[43] although no passage of O_2 through such alternative pathways was observed.

Different free energy isosurfaces, especially the ones at higher free energy contours (e.g., at ΔG = 1 kcal/mol, shown in Fig. 5C), were used to test for the existence of potential O_2 pathways besides the X-ray inferred pathway. However, despite the free energy barriers within the X-ray inferred pathway, the results of flooding simulations show that all of the 39 O_2 molecules reaching the reduction site in cytochrome *aa*$_3$ during the flooding simulations from the solutions (Table 1) use this X-ray inferred pathway, suggesting that the X-ray inferred pathway is the primary O_2 delivery pathway in cytochrome *aa*$_3$.

Delivery rate of O_2

To directly connect the results of the present study to the ones experimentally determined from time-resolved absorption spectroscopy,[32,33] we provide an approximation of the second order rate of O_2 delivery (k_{obs}) to cytochrome *aa*$_3$. Since flooding simulations provide dynamic details of O_2 diffusion, the obtained data can be used to semi-quantitatively describe steps associated with O_2 delivery. The delivery of O_2 to the reduction site involves two major steps: 1) the diffusion of O_2 from the solution to the entrance(s) of the pathway and 2) the migration of O_2 from the entrance(s) to the reduction site. Assuming that the consumption of O_2 is 100% efficient once in the reduction site, k_{obs} can be calculated by using the following steady-state kinetics model:

$$O_2 + E \underset{k_{-1}}{\overset{k_1}{\rightleftharpoons}} E(O_2) \xrightarrow{k_2} E(O_2)_{cat}$$

where $E(O_2)$ is the species in which O_2 has arrived at one of the entrances and $E(O_2)_{cat}$ is when O_2 is in the reduction site. k_{obs} is defined as:

$$k_{obs} = \frac{[O_2]k_1k_2}{[O_2]k_1 + k_{-1} + k_2}.$$

k_1 is the rate constant of O_2 reaching the entrance(s) of the pathway describing the diffusion step of O_2 from the solution to the reduction site. It was calculated as the reciprocal of the product of the time taken to observe the first O_2 molecule diffusing from the solutions to the entrance(s) of the pathway during the simulation (t_{ent}) and the aqueous concentration of O_2

($[O_2]$). The average t_{ent} calculated from all 20 simulations is 2.7 ns and the average $[O_2]$ in the aqueous solution is 67 mM (Table 1), so k_1 is ~5.5×10^9 $M^{-1}s^{-1}$.

k_{-1} is the dissociation rate constant of O_2 from the entrance of the pathway to the membrane. It is the product of k_1 and the standard concentration (1 M) over the partitioning ratio of O_2 at the entrance and the membrane defined as $P_{ent,mem}$). $P_{ent,mem}$ is inversely proportional to exponent of the substraction of ΔG_{ent} from ΔG_{mem}. ΔG_{mem} is ΔG of O_2 in the membrane with respect to the aqueous solution and is −2 to −1.5 kcal/mol.[1,67] ΔG_{ent} is ΔG of O_2 at the entrances of the pathway with respect to the aqueous solution. Because the ΔG contour with ΔG = −3.3 kcal/mol is found at all of the entrances according to ILS calculations (Fig. 5A), ΔG_{ent} is approximated to be −3.3 kcal/mol, indicating that O_2 is 1.3 to 1.8 kcal/mol or 10–20 folds more favored to partition at the entrance of the delivery pathway than in the membrane. Hence, k_{-1} is approximated to be ~$2.8–5.5\times10^8$ s^{-1}.

k_2 is the rate constant of O_2 migration from the entrance(s) to the reduction site and is the reciprocal of the time of O_2 to diffuse into the reduction site after reaching the entrance(s) of the pathway ($t_{cat-ent}$). $t_{cat-ent}$ is obtain by subtracting the time taken to observe the first event of O_2 to the catalytic site or t_{cat}, which is ~57 ns, from t_{ent}. Although the average $t_{cat-ent}$ is 54 ns, O_2 delivery occurred only in 15 out of 20 simulations or 75% of the total number of simulations. To account for this, the average value of $t_{cat-ent}$ was scaled to 72 ns. Thus, k_2 is ~1.39×10^8 s^{-1}.

Under physiologically relevant O_2 concentrations, it is reasonable to assume that $[O_2]$ $k_1 \ll k_{-1}$ and k_2, so

$$k_{obs} \approx \frac{[O_2]k_1k_2}{k_{-1}+k_2}.$$

This leads to the estimated $k_{obs}/[O_2]$ of 1.1–1.8×10^9 $M^{-1}s^{-1}$, which is 8–13 fold slower than the one estimated by our previous MD study with cytochrome ba_3 (15×10^{10} $M^{-1}s^{-1}$).[1] Although this estimated $k_{obs}/[O_2]$ is 10-fold faster than the experimentally determined second-order rate constant of 1×10^8 $M^{-1}s^{-1}$,[32,33] the experimental rate constant was determined from the time required to convert the enzyme from the fully reduced non-O_2 bound state to the ferrous-oxy (O_2 bound) state. Hence, the experimental measurement includes the chemical ligation of O_2 to the heme a_3, the reaction that is beyond to scope of classical MD simulation. The experimental rate constant for O_2 to form the heme Fe adduct in *T.t.* cytochrome ba_3 is 1×10^9 $M^{-1}s^{-1}$,[32,33] which is 10-fold faster than that determined for *R.s.* cytochrome aa_3.

The computationally estimated rate constant for O_2 delivery to the reduction site of cytochrome aa_3 is 1.1×10^9 $M^{-1}s^{-1}$, which means that even when the O_2 concentration is as low as 10 μM, the rate of O_2 diffusion into the reduction site (~10^4 s^{-1}) will be considerably faster than the rate of O_2 catalysis (k_{cat}~10^2 s^{-1}). Because of the specific pathway allowing rapid diffusion of O_2 from the membrane to the reduction site of the enzyme, the rate of catalysis will not be limited by the ambient concentration of O_2 until that concentration in solution is in the low micromolar range.

Constrictions along the O_2 delivery pathway in cytochrome aa_3

Although the O_2 delivery pathway in cytochrome aa_3 contains an additional entrance (Branch C) when compared to cytochrome ba_3, its presence probably has little or no effect on O_2 migration to the reduction site. This is concluded based on previous simulations on cytochrome ba_3 with *in silico* mutants designed to block the two O_2 entrances (Branches A and B in cytochrome ba_3). Those mutants, however, did not appreciably impair the passage of O_2.[1]

Three O_2 entrances of cytochrome aa_3 merge at 12–15 Å distant from the reduction site. At this location, the flooding simulations identified a low O_2 sampling region, which can be seen in the left panel of Fig. 6A. The presence of this barrier region is correlated with a broad range of residence times (1–90 ns) for O_2 in the reduction site (Fig. 3). This region was also characterized by ILS calculations as a diffusion barrier for O_2. The previous study by Oliveira et al[43] also observed this kinetic barrier and, using a similar approach, calculated the energetic cost of ~9.5 kcal/mol for O_2 to pass through this region, thereby excluding the X-ray inferred pathway as the primary O_2 delivery pathway.[43] In the present study, the height of this barrier is suggested to be much smaller since O_2 molecules crossed this region in 15 of 20 150-ns simulations. These results support the role of the X-ray-inferred tunnel as the main, if not the only, pathway used for the substrate O_2 to diffuse to the reduction site.

The region that coincides with the kinetic barrier is surrounded by bulky amino acids M107, W172, F282 and E286 (Fig. 6B, left). This structural feature is common in A-family oxygen reductases. Residue M107 is within TM2, W172 is in the loop connecting TM3 and TM4, and F282 and E286 are both within TM6. W172 and F282 have been suggested to restrict the access of O_2.[24] In cytochrome ba_3, the equivalent region contains amino acids with smaller side chains (Fig. 6B, right), and the barrier height has been estimated to be much less, around 1.5 kcal/mol (Fig. 5C).[1] For example, $M107^{Rs}$ and $F282^{Rs}$ are equivalent to A77 and T231 of cytochrome ba_3, respectively. $W172^{Rs}$ is equivalent to Y133 of cytochrome ba_3, and replaceing this tyrosine by a tryptophan by site-directed mutagenesis resulted in a 5-fold decrease in the O_2 delivery rate.[68] $E286^{Rs}$ is the terminal amino acid of the D channel, a proton-delivery pathway that is present in the A-family HCOs but is absent in B-family HCOs;[26,69] in *T.t* cytochrome ba_3, it is equivalent to I235 (Fig. 6B).

The X-ray inferred pathway in cytochrome aa_3 is not a static pathway, and requires dynamics to change from a closed to an open form to allow for O_2 to migrate across the barrier (Fig. 7 and Fig. S2). Conformational dynamics of the bulky residues of cytochrome aa_3 were assessed by measuring minimum pairwise distances of F282-E286, F282-F108, W172-E286 and M107-E286 (Fig. 7A). The inuences of this dynamics on O_2 migration were examined by ILS calculations over selected periods (Fig. 7B). When the side chains of F282, E286 and M107 protrude into the pathway, they approach each other as well as F108 and W172, significantly interfering with O_2 migration. For example, during the 171–175 ns period of the 200-ns apo simulation in which all of the four distances came close to 4 Å, the free energy for O_2 to migrate through the kinetic barrier can be greater than 4 kcal/mol (Fig. 7B). As indicated in Fig. 7A, the occurrence of these conformational changes, however, is relatively infrequent and might not be observed using shorter simulation times.

Finally, it is noted that, in the A-family HCOs, both pumped and chemical protons pass from the D channel to the periplasmic surface and the reduction site via hydrogen-bonded water chains. The terminal region of the O_2 delivery pathway is also overlapped to that of the D channel. Since chemical protons and O_2 use the same delivery route to the reduction site, the presence of transiently localized water molecules may interfere with the passage of O_2. However, in the simulations performed in the present study as well as those reported in the recent study by Oliveira et al,[43] the region connecting the terminus of the D channel and the reduction site remained dehydrated. Therefore, we can only conclude that the observed restriction of O_2 migration is related to the presence of amino acids with bulky side chain. The transient presence of water in this region could also affect the rate of O_2 delivery in the A-family HCOs which possess the D channel.

Conclusion

This MD study characterizes the X-ray inferred tunnel as the primary delivery pathway for O_2 in *R.s.* cytochrome aa_3. This conclusion is opposite to the one made by Oliviera et al, likely related to shorter simulation times used in the previous study[43] due to slow conformational dynamics of amino acids lining the pathway. Because there are multiple constriction regions along the pathway indicated by both flooding simulations and ILS calculations, the simulation time needs to be sufficiently long to observe the migration of O_2 to the reduction site of *R.s.* cytochrome aa_3. We conclude that both *R.s.* cytochrome aa_3 and *T.t.* cytochrome ba_3 use similar pathways to effectively deliver O_2, and this pathway also appears to be conserved in other HCOs.

Supplementary Material

Refer to Web version on PubMed Central for supplementary material.

Acknowledgments

The authors acknowledge funding supports from the National Institutes of Health (NIH P41-GM104601, U01-GM111251 and U54-GM087519 to E.T., and R01-HL16101 to R.B.G.) and the Office of Naval Research (ONR N00014-16-1-2535 to E.T.). P.M. gratefully acknowledges NIH support as a trainee of the Molecular Biophysics Training Program (5T32-GM008276) during his graduate study. Computational resources were provided by XSEDE (XSEDE MCA06N060) and Blue Waters (ACI-1440026).

References

1. Mahinthichaichan P, Gennis R, Tajkhorshid E. All the O_2 consumed by *Thermus thermophilus* cytochrome $ba_3$is delivered to the active site through a long, open hydrophobic tunnel with entrances within the lipid bilayer. Biochemistry. 2016; 55:1265–1278. [PubMed: 26845082]
2. Pereira M, Santana M, Teixeira M. A novel scenario for the evolution of haem-copper oxygen reductases. Biochim. Biophys. Acta – Bioener. 2001; 1505:185–208.
3. Sousa FL, Alves RJ, Ribeiro MA, Pereira-Leal JB, Teixeira M, Pereira MM. The superfamily of heme-copper oxygen reductases: Types and evolutionary considerations. Biochim. Biophys. Acta – Bioener. 2012; 1817:629–637.
4. Morris RL, Schmidt T. Shallow breathing: bacteria life at low O_2. Nat. Rev. Microbiol. 2013; 11:205–212. [PubMed: 23411864]
5. Wikström M, Sharma V, Kaila VR, Hosler JP, Hummer G. New Perspective on Proton Pumping in Cellular Respiration. Chem. Rev. 2015; 115:2196–2221. [PubMed: 25694135]

6. Babcock G, Wikström M. Oxygen activation and the conservation of energy in cell respiration. Nature. 1992; 256:301–309.
7. Ferguson-Miller S, Babcock GT. Heme/Copper Terminal Oxidases. Chem. Rev. 1996; 96:2889. [PubMed: 11848844]
8. Hosler JP, Ferguson-Miller S, Mills DA. Energy Transduction: Proton Transfer Through the Respiratory Complexes. Annu. Rev. Biochem. 2006; 75:165–187. [PubMed: 16756489]
9. Kaila VR, Verkhovsky MI, Wikström M. Proton-coupled electron transfer in cytochrome oxidase. Chem. Rev. 2010; 110:7062–7082. [PubMed: 21053971]
10. Brzezinski P, Gennis RB. Cytochrome c oxidase: exciting progress and remaining mysteries. J. Bioenerg. Biomembr. 2008; 40:521–531. [PubMed: 18975062]
11. Rich PR, Marechal A. Functions of the hydrophilic channels in proton-motive cytochrome *c* oxidase. J. R. Soc. Interface. 2013; 10:20130183. [PubMed: 23864498]
12. Ducluzeau AL, Schoepp-Cothenet B, van Lis R, Baymann F, Russell MJ, Nitschke W. The evolution of respiratory O_2/NO reductases: an out-of-the-phylogenetic-box perspective. J. R. Soc. Interface. 2014; 11:20140196. [PubMed: 24968694]
13. Svensson-Ek M, Abramson J, Larsson G, Törnroth S, Brzezinski P, Iwata S. The X-ray Crystal Structures of Wild-type and EQ(I-286) Mutant Cytochrome c Oxidases from *Rhodobacter sphaeroides*. J. Mol. Biol. 2002; 321:329–339. [PubMed: 12144789]
14. Qin L, Hiser C, Mulichak A, Garavito RM, Ferguson-Miller S. Identification of conserved lipid/detergent-binding sites in a high-resolution structure of the membrane protein cytochrome c oxidase. Proc. Natl. Acad. Sci. USA. 2006; 103:16117–16122. [PubMed: 17050688]
15. Ostermeier C, Harrenga A, Ermler U, Michel H. Structure at 2.7 Å resolution of the *Paracoccus denitrificans* two-subunit cytochrome c oxidase complexed with an antibody FV fragment. Proc. Natl. Acad. Sci. USA. 1997; 94:10547. [PubMed: 9380672]
16. Tsukihara T, Aoyama H, Yamashita E, Tomizaki T, Yamaguchi H, Shinnzawha-Itoh K, Nakashima R, Yaono R, Yoshikawa S. The Whole Structure of the 13-Subunit Oxidized Cytochrome c Oxidase at 2.8 Å. Science. 1996; 272:1136–1144. [PubMed: 8638158]
17. Yoshikawa S, Shinzawaitoh K, Nakashima R, Yaono R, Yamashita E, Inoue N, Yao M, Fei MJ, Libeu CP, Mizushima T, Yamaguchi H, Tomizaki T, Tsukihara T. Redox-coupled crystal structural changes in bovine heart cytochrome *c* oxidase. Science. 1998; 280:1723–1729. [PubMed: 9624044]
18. Tsukihara T, Shimokata K, Katayama Y, Shimada H, Muramoto K, Aoyama H, Mochizuki M, Shizawa-Itoh K, Yamashita E, Yao M, Ishimura Y, Yoshikawa S. The low-spin heme of cytochrome c oxidase as the driving element of the proton-pumping process. Proc. Natl. Acad. Sci. USA. 2003; 100:15304–15309. [PubMed: 14673090]
19. Shinzawa-Itoh K, Aoyama H, Muramoto K, Terada H, Kurauchi T, Tadehara Y, Yamasaki A, Sugimura T, Kurono S, Tsujimoto K, Mizushima T, Yamashita E, Tsukihara T, Yoshikawa S. Structures and physiological roles of 13 integral lipids of bovine heart cytochrome c oxidase. EMBO J. 2007; 26:1713–1725. [PubMed: 17332748]
20. Abramson J, Svensson-Ek M, Byrne B, Iwata S. Structure of cytochrome *c* oxidase: a comparison of the bacterial and mitochondrial enzymes. Biochim. Biophys. Acta. 2001; 1544:1–9. [PubMed: 11341911]
21. Yoshikawa S, Shimada A. Reaction Mechanism of Cytochrome c Oxidase. Chem. Rev. 2015; 115:1936–1989. [PubMed: 25603498]
22. Abramson J, Riistama S, Larsson G, Jasaitis A, Svensson-Ek M, Laakkonen L, Puustinen A, Iwata S, Wikström M. The structure of the ubiquinol oxidase from *Escherichia coli* and its ubiquinone binding site. Nat. Struct. Biol. 2000; 7:910–917. [PubMed: 11017202]
23. Musser SM, Stowell MH, Chan SI. Comparison of ubiquinol and cytochrome *c* terminal oxidases: An alternative view. FEBS Lett. 1993; 327:131–136. [PubMed: 8392948]
24. Luna VM, Chen Y, Fee JA, Stout CD. Crystallographic Studies of Xe and Kr Binding within the Large Internal Cavity of Cytochrome ba_3 from *Thermus thermophilus*: Structural Analysis and Role of Oxygen Transport Channels in the Heme-Cu Oxidases. Biochemistry. 2008; 47:4657–4665. [PubMed: 18376849]

25. Luna VM, Fee JA, Deniz AA, Stout CD. Mobility of Xe Atoms within the Oxygen Diffusion Channel of Cytochrome ba_3 Oxidase. Biochemistry. 2012; 51:4669–4676. [PubMed: 22607023]
26. Soulimane T, Buse G, Bourenkov GP, Bartunik HD, Huber R, Than ME. Structure and mechanism of the abberrant ba_3-cytochrome c oxidase from *Thermus thermophilus*. EMBO J. 2000; 19:1766–1776. [PubMed: 10775261]
27. Hunsicker-Wang L, Pacoma R, Chen Y, Fee J, Stout C. A novel cryoprotection scheme for enhancing the diffraction of crystals of recombinants cytochrome ba_3 oxidase from *Thermus thermophilus*. Acta Cryst. D. 2005; 61:340–343. [PubMed: 15735345]
28. Tiefenbrunn T, Liu W, Chen Y, Katritch V, Stout CD, Fee JA, Cherezov V. High Resolution Structure of the ba_3 Cytochrome c Oxidase from *Thermus thermophilus* in a Lipidic Environment. PLoS One. 2011; 6:e22348. [PubMed: 21814577]
29. Iwata S, Ostermeier C, Ludwig B, Michel H. Structure at 2.8 Å Resolution of Cytochrome *C* Oxidase From *Paracoccus denitrificans*. Nature. 1995; 376:660–669. [PubMed: 7651515]
30. Tsukihara T, Aoyama H, Yamashita E, Tomizaki T, Yamaguchi H, Shinnzawha-Itoh K, Nakashima R, Yaono R, Yoshikawa S. Structures of Metal Sites of Oxidized Bovine Heart Cytochrome C Oxidase at 2.8 Å. Science. 1995; 269:1069–1074. [PubMed: 7652554]
31. Lyons JA, Aragao D, Slattery O, Pisliakov AV, Soulimane T, Caffrey M. Structural insights into electron transfer in caa_3-type cytochrome oxidase. Nature. 2012; 487:514–518. [PubMed: 22763450]
32. Szundi I, Funatogawa C, Fee JA, Soulimane T, Einarsdóttir O. CO impedes superfast O_2 binding in ba_3 cytochrome oxidase from *Thermus thermophilus*. Proc. Natl. Acad. Sci. USA. 2010; 107:21010–21015. [PubMed: 21097703]
33. Einarsdóttir O, Funatogawa C, Soulimane T, Szundi I. Kinetic studies of the reactions of O_2 and NO with reduced *Thermus thermophilus* ba_3 and bovine aa_3 using photolabile carriers. Biochim. Biophys. Acta – Bioener. 2012; 1817:672–679.
34. Hosler JP. The inuence of subunit III of cytochrome *c* oxidase on the D pathway, the proton exit pathway and mechanism-based inactivation in subunit I. Biochim. Biophys. Acta. 2004; 1655:332–339. [PubMed: 15100048]
35. Varansi L, Hosler JP. Subunit III-depleted cytochrome *c* oxidase provides insight into the process of proton uptake by proteins. Biochim. Biophys. Acta – Bioener. 2012; 1817:545–551.
36. Mills DA, Hosler JP. Slow Proton Transfer through the Pathways for Pumped Protons in Cytochrome *c* Oxidase Induces Suicide Inactivation of the Enzyme. Biochemistry. 2005; 44:4656–4666. [PubMed: 15779892]
37. Mills DA, Tan Z, Ferguson-Miller S, Hosler J. A Role for Subunit III in Proton Uptake into the D Pathway and a Possible Proton Exit Pathway in *Rhodobacter sphaeroides* Cytochrome *c* Oxidase. Biochemistry. 2003; 42:7410–7417. [PubMed: 12809496]
38. Qin L, Sharpe MA, Garavito RM, Ferguson-Miller S. Conserved lipid-binding sites in membrane proteins: a focus on cytochrome c oxidase. Curr. Opin. Struct. Biol. 2007; 17:444–450. [PubMed: 17719219]
39. Qin L, Mills DA, Buhrow L, Hiser C, Ferguson-Miller. A Conserved Steroid Binding Site in Cytochrome *c* Oxidase. Biochemistry. 2008; 47:9931–9933. [PubMed: 18759498]
40. Qin L, Liu J, Mills DA, Proshlyakov DA, Hiser C, Ferguson-Miller S. Redox-Dependent Conformational Changes in Cytochrome *c* Oxidase Suggest a Gating Mechanism for Proton Uptake. Biochemistry. 2009; 48:5121–5130. [PubMed: 19397279]
41. Hofacker I, Schulten K. Oxygen and Proton Pathways in Cytochrome *c* Oxidase. Proteins: Struct., Func., Gen. 1998; 30:100–107.
42. Elber R, Karplus M. Enhanced Sampling in Molecular Dynamics: Use of the Time-Dependent Hartree Approximation for a Simulation of Carbon Monoxide Diffusion through Myoglobin. J. Am. Chem. Soc. 1990; 112:9161–9175.
43. Oliveira AS, Damas JM, Baptista A, Soares CM. Exploring O_2 diffusion in A-type cytochrome c oxidases: molecular dynamics simulations uncover two alternative channels towards the binuclear site. PLoS Comput. Biol. 2014; 10:e1004010. [PubMed: 25474152]
44. Cohen J, Arkhipov A, Braun R, Schulten K. Imaging the migration pathways for O_2, CO, NO, and Xe inside myoglobin. Biophys. J. 2006; 91:1844–1857. [PubMed: 16751246]

45. Riistama S, Puustinen A, Verkhovsky MI, Morgan JE, Wikström M. Binding of O_2 and Its Reduction Are Both Retarded by Replacement of Valine 279 by Isoleucine in Cytochrome c Oxidase from *Paracoccus denitrificans*. Biochemistry. 2000; 39:6365–6372. [PubMed: 10828950]
46. Riistama S, Puustinen A, García-Horsman A, Iwata S, Michel H, Wikström M. Channelling of dioxygen into the respiratory enzyme. Biochim. Biophys. Acta. 1996; 1275:1–4. [PubMed: 8688439]
47. Chovancova E, Pavelka A, Benes P, Strnad O, Brezovsky J, Kozlikova B, Gora A, Sustr V, Klvana M, Medek P, Biedermannova L, Sochor J, Damborsky J. CAVER 3.0: A Tool for the Analysis of Transport Pathways in Dynamic Protein Structures. PLoS Comput. Biol. 2012; 8:e1002708. [PubMed: 23093919]
48. Humphrey W, Dalke A, Schulten K. VMD – Visual Molecular Dynamics. J. Mol. Graphics. 1996; 14:33–38.
49. Namslauer A, Aagaard A, Katsonouri A, Brzezinski P. Intromolecular Proton-Transfer Reactions in a Membrane-Bound Proton Pump: The Effect of pH on the Peroxy to Ferryl Transition in Cytochrome *c* Oxidase. Biochemistry. 2003; 42:1488–1498. [PubMed: 12578361]
50. Lomize MA, Lomize AL, Pogozheva LD, Mosberg HI. OPM: Orientations of Proteins in Membranes database. Bioinformatics. 2006; 22:623–625. [PubMed: 16397007]
51. Lomize MA, Pogozheva ID, Joo H, Mosberg HI, Lomize AL. OPM database and PPM web server: resources for positioning of proteins in membranes. Nucleic Acids Res. 2012; 40:D370–376. [PubMed: 21890895]
52. MacKerell AD Jr, et al. All-atom empirical potential for molecular modeling and dynamics studies of proteins. J. Phys. Chem. B. 1998; 102:3586–3616. [PubMed: 24889800]
53. MacKerell AD Jr, Feig M, Brooks CL III. Extending the Treatment of Backbone Energetics in Protein Force Fields: Limitations of Gas-Phase Quantum Mechanics in Reproducing Protein Conformational Distributions in Molecular Dynamics Simulations. J. Comp. Chem. 2004; 25:1400–1415. [PubMed: 15185334]
54. Klauda JB, Venable RM, Freites JA, O'Connor JW, Tobias DJ, Mondragon-Ramirez C, Vorobyov I, MacKerell AD Jr, Pastor RW. Update of the CHARMM all-atom additive force field for lipids: Validation on six lipid types. J. Phys. Chem. B. 2010; 114:7830–7843. [PubMed: 20496934]
55. Jorgensen WL, Chandrasekhar J, Madura JD, Impey RW, Klein ML. Comparison of simple potential functions for simulating liquid water. J. Chem. Phys. 1983; 79:926–935.
56. Fuchs J-F, Nedev H, Poger D, Ferrand M, Brenner V, Dognon J-P, Crouzy S. New model potentials for sulfur-copper(I) and sulfur-mercury(II) interactions in proteins: From *ab initio* to molecular dynamics. J. Comp. Chem. 2006; 27:837–856. [PubMed: 16541427]
57. Vanommeslaeghe K, Hatcher E, Acharya C, Kundu S, Zhong S, Shim J, Darian E, Guvench O, Lopes P, Vorobyov I, MacKerell AD Jr. CHARMM General Force Field: A Force Field for Drug-Like Molecules Compatible with the CHARMM All-Atom Additive Biological Force Fields. J. Comp. Chem. 2010; 31:671–690. [PubMed: 19575467]
58. Phillips JC, Braun R, Wang W, Gumbart J, Tajkhorshid E, Villa E, Chipot C, Skeel RD, Kale L, Schulten K. Scalable Molecular Dynamics with NAMD. J. Comp. Chem. 2005; 26:1781–1802. [PubMed: 16222654]
59. Ryckaert J-P, Ciccotti G, Berendsen HJC. Numerical Integration of the Cartesian Equations of Motion of a System with Constraints: Molecular Dynamics of *n*-Alkanes. J. Comp. Phys. 1977; 23:327–341.
60. Darden T, York D, Pedersen LG. Particle mesh Ewald: An $N\cdot\log(N)$ method for Ewald sums in large systems. J. Chem. Phys. 1993; 98:10089–10092.
61. Martyna GJ, Tobias DJ, Klein ML. Constant Pressure Molecular Dynamics Algorithms. J. Chem. Phys. 1994; 101:4177–4189.
62. Feller SE, Zhang Y, Pastor RW, Brooks BR. Constant pressure molecular dynamics simulation: The Langevin piston method. J. Chem. Phys. 1995; 103:4613–4621.
63. Daigle R, Guertin M, Lague P. Structural characterization of the tunnels of *Mycobacterium tuberculosis* truncated hemoglobin N from molecular dynamics simulations. Proteins: Struct., Func., Bioinf. 2009; 75:735–747.

64. Wang Y, Cohen J, Boron WF, Schulten K, Tajkhorshid E. Exploring Gas Permeability of Cellular Membranes and Membrane Channels with Molecular Dynamics. J. Struct. Biol. 2007 In press.

65. Wang Y, Tajkhorshid E. Nitric oxide conduction by the brain aquaporin AQP4. Proteins: Struct., Func., Bioinf. 2010; 78:661–670.

66. Frenkel, D., Smit, B. Understanding Molecular Simulation From Algorithms to Applications. Academic Press; California: 2002.

67. Wang Y, Tajkhorshid E. Molecular Mechanisms of Conduction and Selectivity in Aquaporin Water Channels. J. Nutr. 2007; 137:1509S–1515S. [PubMed: 17513417]

68. McDonald W, Funatogawa C, Li Y, Szundi I, Fee YCA, Stout CD, Einarsdóttir O. Ligand access to the active site in *Thermus thermophilus* ba_3 and bovine heart aa_3 cytochrome oxidases. Biochemistry. 2013; 52:640–652. [PubMed: 23282175]

69. Chang HY, Hemp J, Chen Y, Fee JA, Gennis RB. The cytochrome ba_3 oxygen reductase from *Thermus thermophilus* uses a single input channel for proton delivery to the active site and for proton pumping. Proc. Natl. Acad. Sci. USA. 2009; 106:16169–16173. [PubMed: 19805275]

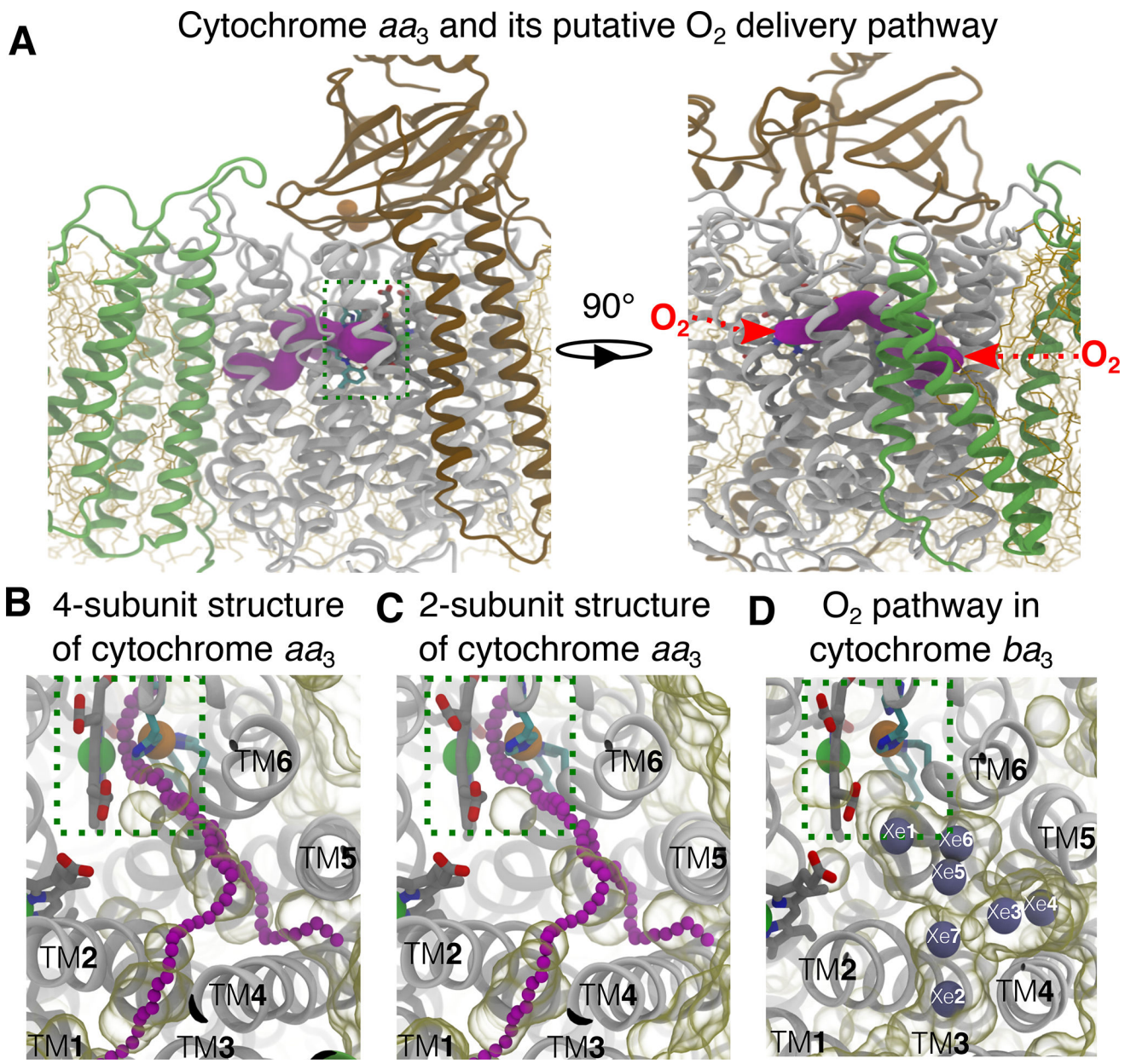

Figure 1.

Putative O_2 delivery pathway in HCOs. A) Location of the pathway in cytochrome *aa*$_3$. The *R.s.* enzyme comprises four subunits: SI (white), SII (brown), SIII (green) and SIV (not shown). SI and SII are the minimal functional units of HCOs. The O_2 reduction site is highlighted using a dashed green box. The X-ray inferred pathway, located in SI, is shown in magenta surface drawn using CAVER 3.0.[47] This structural model is from PDB 1M56.[13] Red arrows on the right panel depict the entrances of the pathway. B–C) Projected from the top view, the putative O_2 pathway in cytochrome *aa*$_3$ is illutrated by chains of magenta balls drawn by CAVER3.0. Unoccupied spaces within the protein were visualized using the molecular surface representation in VMD with the probe radius of 1.7 Å, which is about the vdW radius of an oxygen atom. Comparison between the crystal structure with 4 subunits

(B) and the one with only SI and SI subunits from PDB 2GSM[14] (C) indicates that SIII does not block the TM4–5 entrance. The simulations were performed using the 2-subuit structure. D) The equivalent pathway in cytochrome ba_3 was found to bind Xe (gray balls) by X-ray crystallographic experiments[24,25] and characterized as the O_2 delivery pathway in MD simulations.[1] The structural model is from PDB 1XME[27] and the atom coordinates of Xe are from PDB 3BVD.[24] The Xe atoms are numbered according to Luna et al.[24]

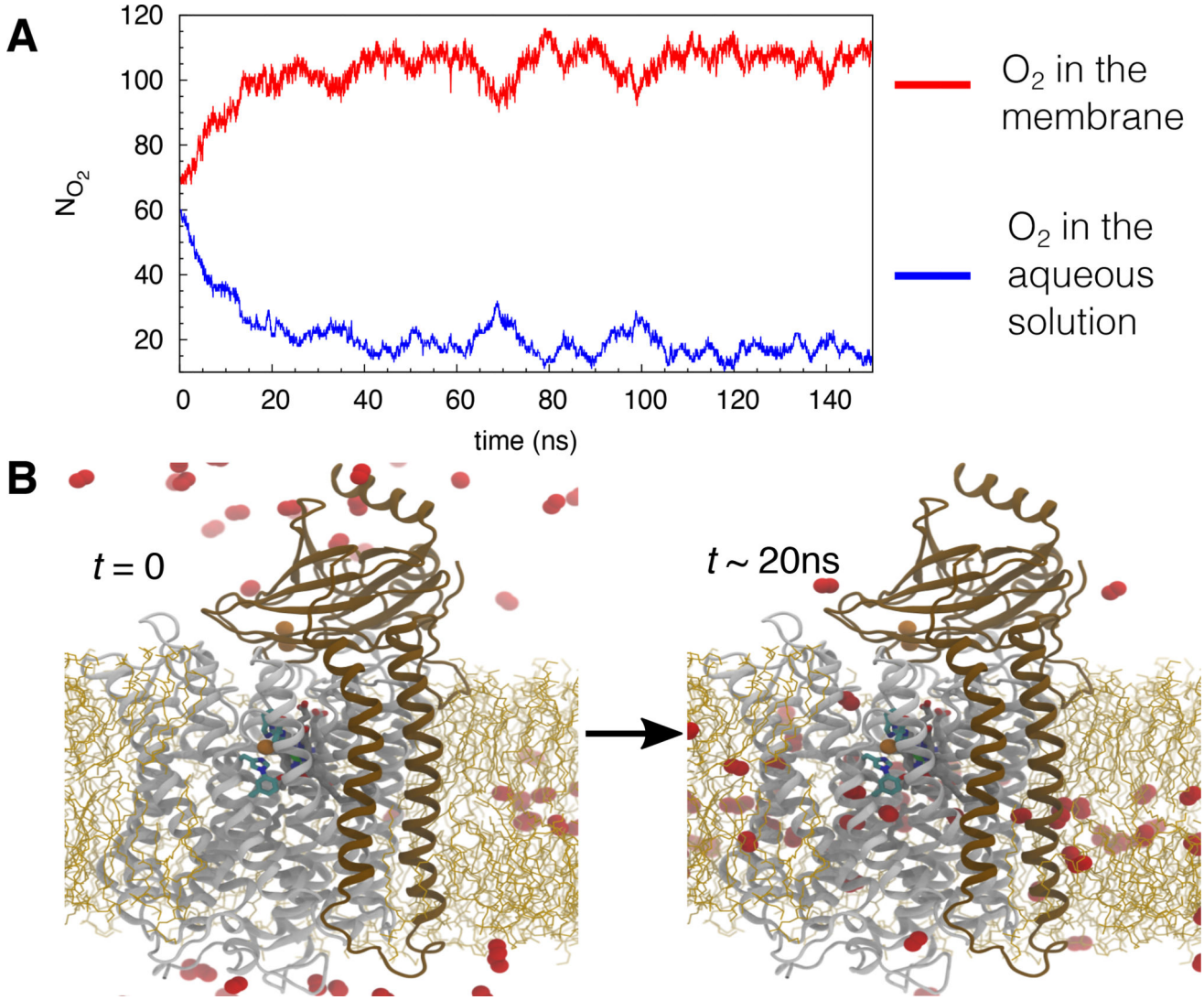

Figure 2.

Flooding simulations of O_2 diffusion in the membrane-embedded cytochrome *aa*$_3$. A) An example taken from one of the simulation illustrating the number of O_2 molecules (N_{O2}) localized in the membrane and in the aqueous solution. At the beginning of the simulation, 70 O_2 molecules were placed in the membrane and 60 in the aqueous solution. After reaching the equilibrium, ~110 O_2 molecules localized in the membrane and ~20 localized in the aqueous solution. B) Snapshots taken from one of the simulations illustrating the starting (left) and equilibrium points. Helices shown in white belong to SI, while ones shown in brown belong to SII. Lipid molecules are shown in orange sticks.

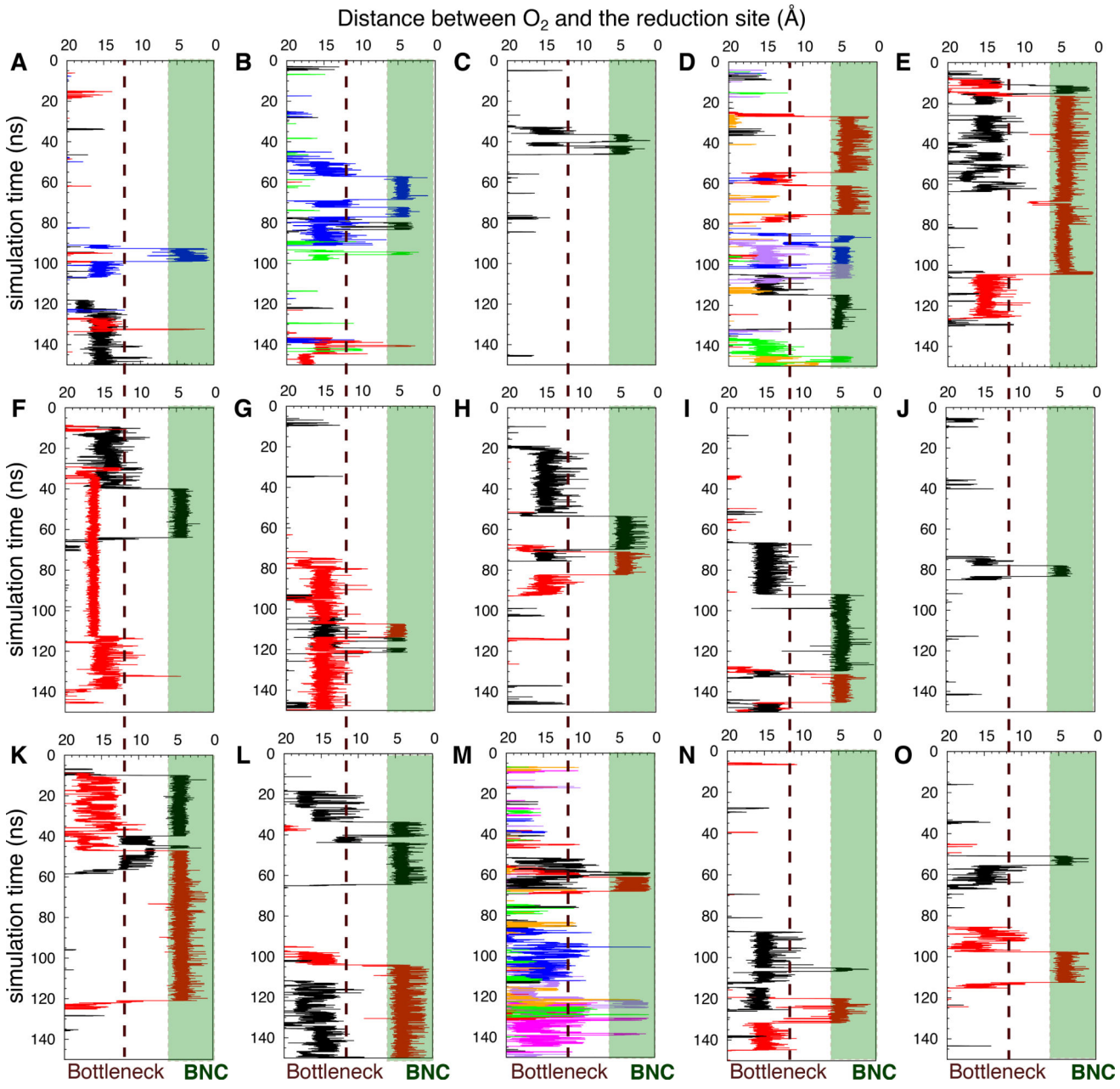

Figure 3.

Access of O_2 to the reduction site during 150-ns timespan of the simulations quantified by the distance between an O_2 molecule and the binuclear center (denoted as BNC) of the reduction site (O_2-cat) as the function of simulation time. Each panel represents one of the 15 simulations in which O_2 delivery took place. In relation to Table 1, panels A–D denote Sims. 1A–D, panels E–H denote Sims. 2A–D, panels I–K denote Sims. 3A and 3D–E, and panels L–O denote Sims. 4A–B and 4D–E. Each line corresponds to the trajectory of an individual O_2 molecule diffusing into the reduction site (shaded green), defined by the proximity of <6 Å from the centers of mass between the Fe atom of heme a_3 and Cu_B. The dashed line in each panel indicates the location of the main bottleneck, corresponding to the

kinetic barrier region separating the reduction site from the rest of the O_2 delivery pathway, where O_2 resided very transiently while diffusing towards the reduction site.

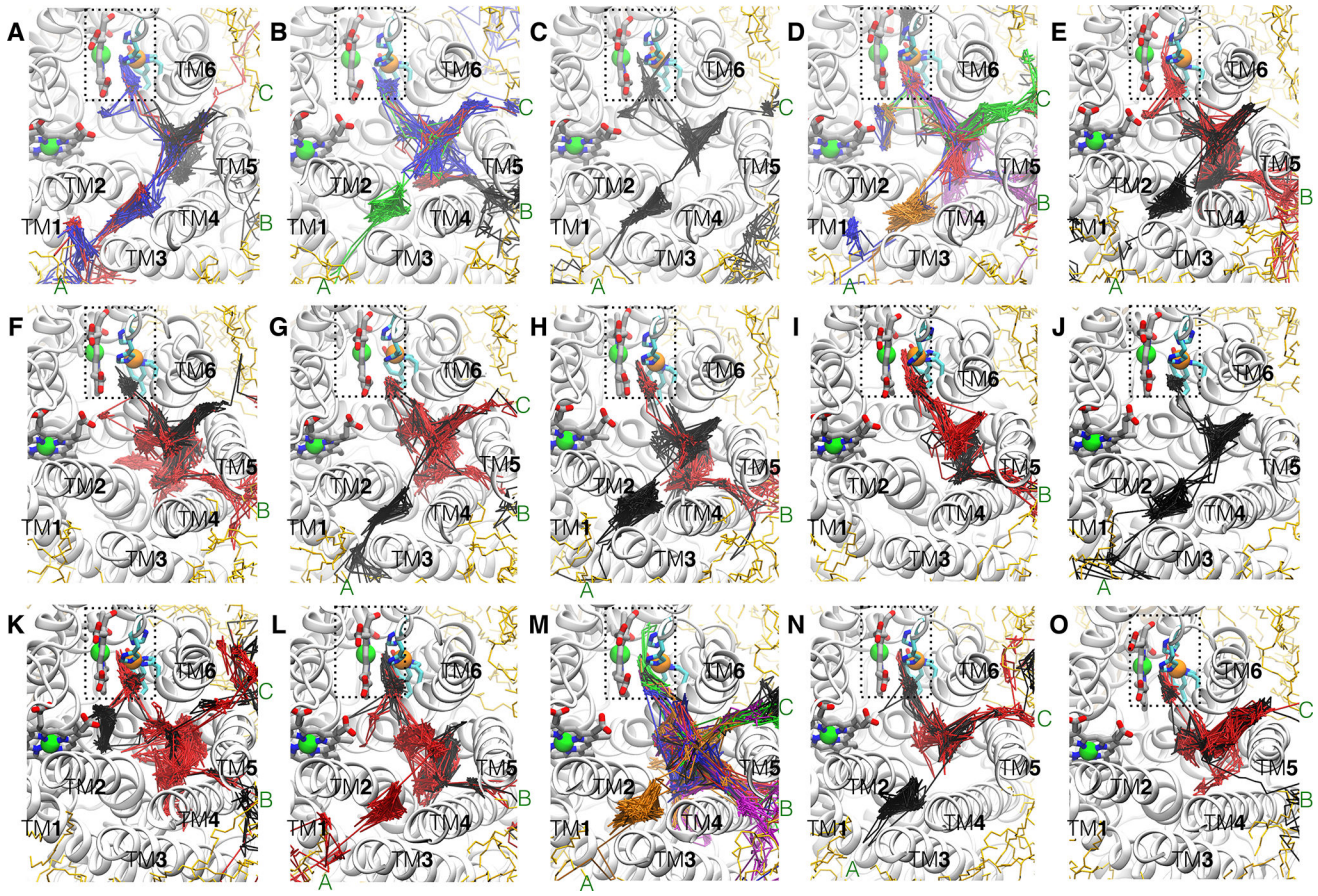

Figure 4.

O_2 access routes. The trajectories of the delivered O_2 molecules into the reduction site during each of the 15 simulations are illustrated by line traces with different colors. O_2 molecules enter the X-ray inferred pathway via three membrane-accessible branches, denoted as “A”, “B” and “C”. Branch A originates at TM1, TM2 and TM3. Branch B originates at TM4 and TM5 which is adjacent to SIII. Branch C, which was previously unknown, originates at TM5 and TM6. In some of the simulations, O_2 were found entering via all 3 branches, whereas in others, they entered via only 1 or 2 of the branches were visited by O_2. In relation to Table 1, panels A–D denote Sims. 1A–D, panels E–H denote Sims. 2A–D, panels I–K denote Sims. 3A and 3D–E, and panels L–O denote Sims. 4A–B and 4D–E.

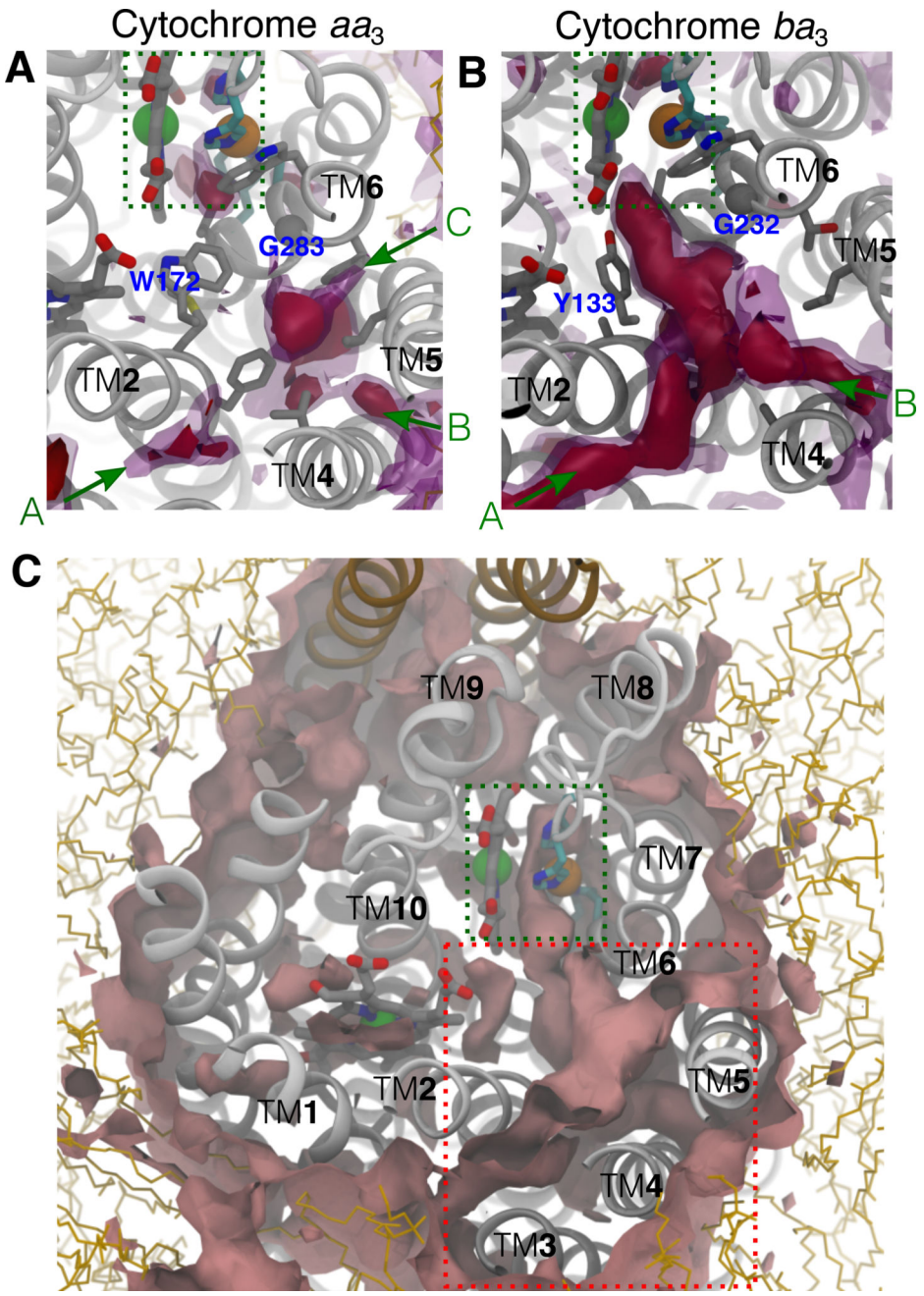

Figure 5.

Potential O_2 pathways predicted by ILS. A) Equivalent regions to the O_2 delivery pathway of cytochrome aa_3. Red isosurfaces correspond to ΔG of ~-3.3 kcal/mol. Magenta isosurfaces correspond to ΔG ~-1.8 kcal/mol. Discontinuous gaps between the isosurfaces indicate unfavorable O_2 insertion regions, correlated with hindrances along the pathway. Constricting residues are labeled; E286 (not shown) is located below F282 and G283. B) The entire pathway of cytochrome ba_3 is highly favorable for O_2. The ILS results of cytochrome ba_3 were obtained by analyzing the simulation trajectories for our previous study.[1] C) Other potential O_2 delivery pathways in cytochrome aa_3. Pink surfaces

correspond to ΔG of +1 kcal/mol. The O_2 pathway, highlighted in dashed red box, is the only region extending all the way from the membrane to the reduction site. The alternate pathways proposed by Oliveira et al[43] start in between TM7 and TM8 and in between SII (brown), TM8 and TM9.

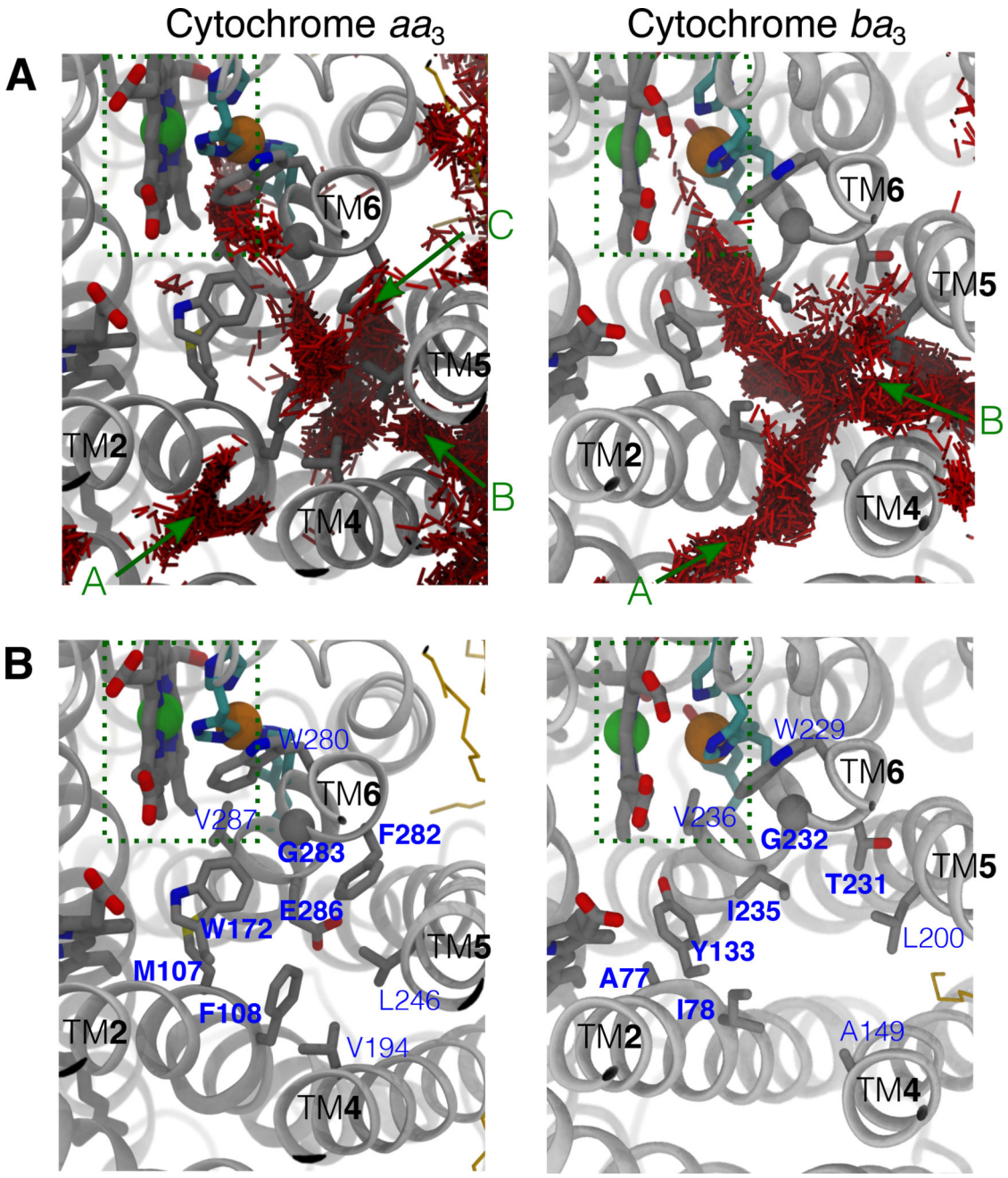

Figure 6.

Constricting residues along the O_2 delivery pathway of cytochrome aa_3. A) Occupancy of O_2 in cytochrome aa_3 (left) vs. cytochrome ba_3 (right). Red lines are the collections of O_2 molecules partitioning in the protein during a flooding simulation (150 ns for aa_3 and 50 ns for ba_3). The results of cytochrome ba_3 were taken from the simulation trajectories performed in our previous study.[1] B) Comparison of amino acid residues lining the pathway in cytochrome aa_3 (left) and cytochrome ba_3 (right). Constricting residues, which surround the kinetic barrier region of the O_2 delivery pathway in cytochrome aa_3 are labeled in bold; their equivalences in cytochrome aa_3 are also labeled in bold.

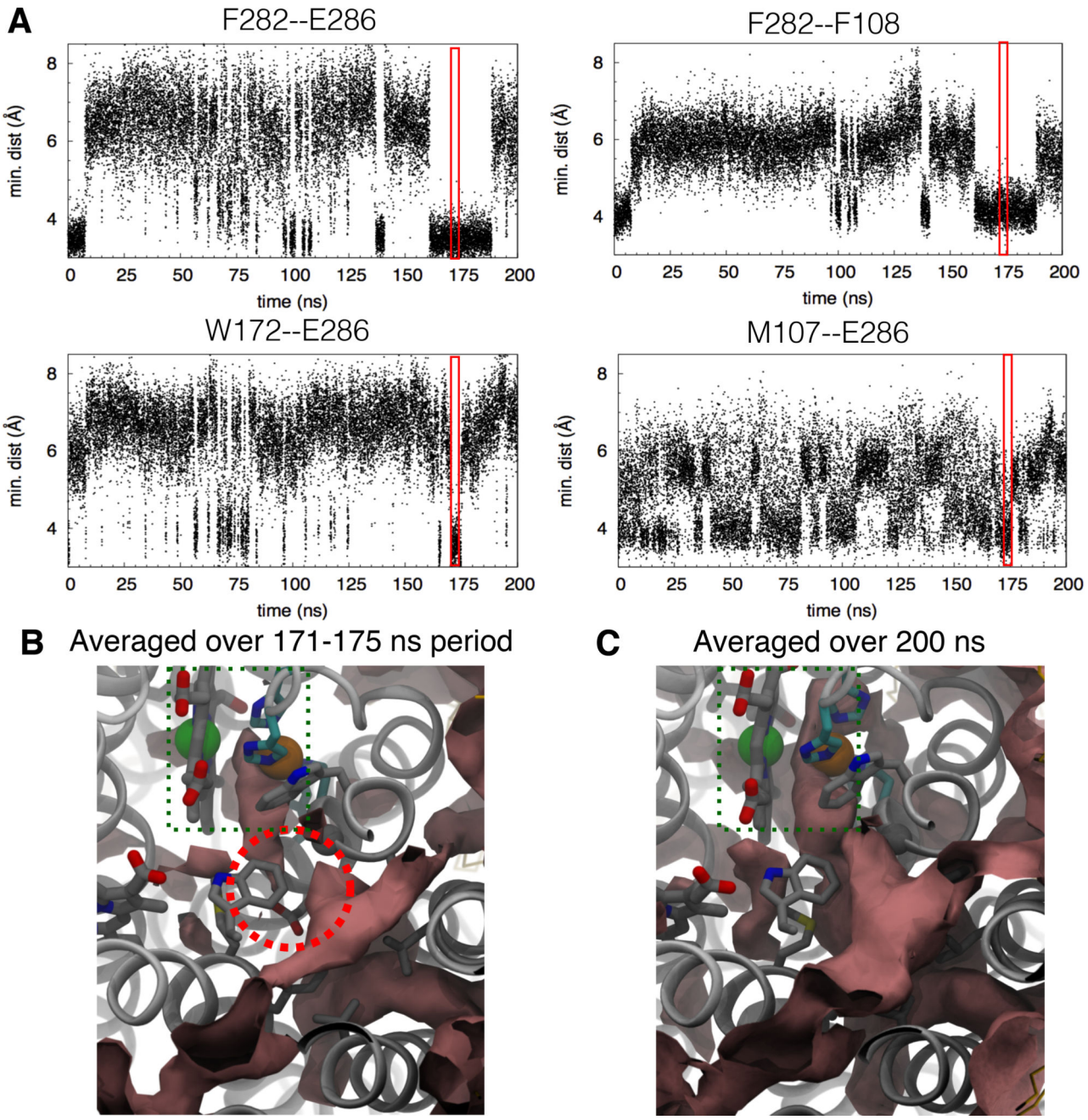

Figure 7.

Conformational dynamics of constricting residues and O_2 accessibility. A) Minimum distances between lining amino acid residues during the 200-ns apo simulation. Dynamics of the residues affects O_2 passage. For example, from 171 to 175 ns (highlighted in red), the side chain of E286 comes in contact with those of W172, M107 and F108, while that of F282 comes very close to that of F108. These close contacts restrict O_2 passage. In the crystal structures, N-C_α-C_β-C_γ of F282 is ~180° which constricted the pathway; its transition to 60° increases its contact distances to E286 and F108 from 4 to 6 Å, relieving the hindrance. Residue F108 is located opposite to F282 and in cytochrome ba_3, it is

equivalent to residue I78 (Fig. 6B) B) ΔG isosurface of +1 kcal/mol (pink surfaces) calculated using ILS over the period from 171 to 175 ns. The kinetic barrier is encircled in red, indicating a high energy of O_2 insertion and the blockage of O_2 passage. C) ΔG isosurface of +1 kcal/mol calculated over the entire 200-ns trajectory. Referring to Fig. 5A, ΔG of the two regions adjacent to the barrier are lower than −3.3 kcal/mol indicated in red surfaces. Hence, the ΔG barrier is greater than 4 kcal/mol when the constricting residues simultaneously form very close contacts.

Table 1

Access of O_2 to the reduction site of cytochrome aa_3

Sim.	No. entry events	t_{cat} (ns)	Bulk <[O_2] >	t_{ent} (ns)	$t_{cat-ent}$ (ns)
1A	3	92.6	57 mM	2.11	90.49
1B	4	57.15	63 mM	6.84	50.31
1C	1	36.45	60 mM	2.59	33.86
1D	6	27.02	71 mM	3.28	23.74
1E	0	NA	63 mM	3.91	NA
2A	2	11.45	70 mM	1.93	9.52
2B	2	39.95	69 mM	0.34	39.61
2C	2	107.38	74 mM	0.63	106.75
2D	2	53.48	70 mM	4.38	49.1
2E	0	NA	73 mM	2.23	NA
3A	2	91.95	68 mM	1.72	90.23
3B	0	NA	74 mM	4.04	NA
3C	0	NA	70 mM	0.62	NA
3D	1	78.01	70 mM	4.38	73.63
3E	2	9.97	60 mM	1.94	8.03
4A	2	33.7	62 mM	2.5	31.2
4B	7	58.74	62 mM	0.82	57.92
4C	0	NA	64 mM	3.85	NA
4D	2	105.03	65 mM	2.26	102.77
4E	2	50.94	81 mM	2.77	48.17
Avg.	**2**	**57**	**67 mM**	**2.7**	**54**

t_{cat} is the time taken to observe the first entry event of O_2 to the reduction site. t_{ent} is the time taken to observe the first O_2 molecule reaching the entrance(s) of the O_2 delivery pathway. Sims 1X, 2X, 3X and 4X were prepared using the 25-ns, 100-ns, 150-ns and 200-ns equilibrated complex of the 200-ns apo simulation as the starting model.